Electronic Supplementary Material (ESI) for Journal of Materials Chemistry C.
This journal is © The Royal Society of Chemistry 2023

Supplementary Information

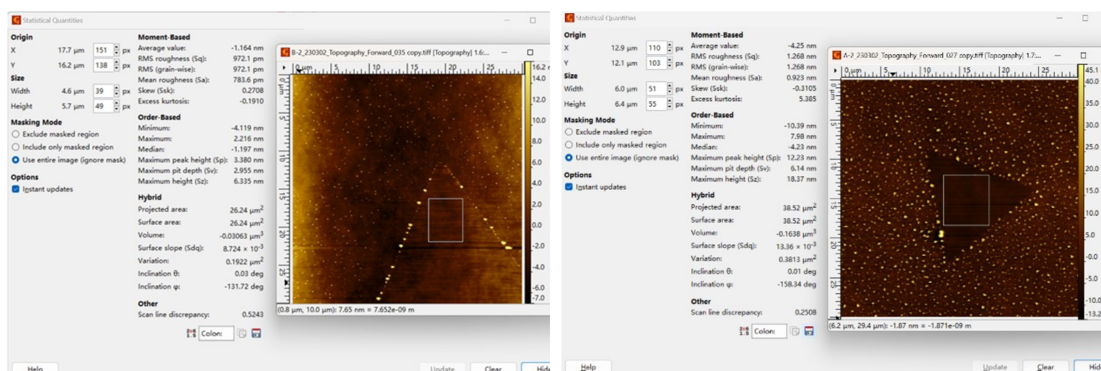

(a) (b)

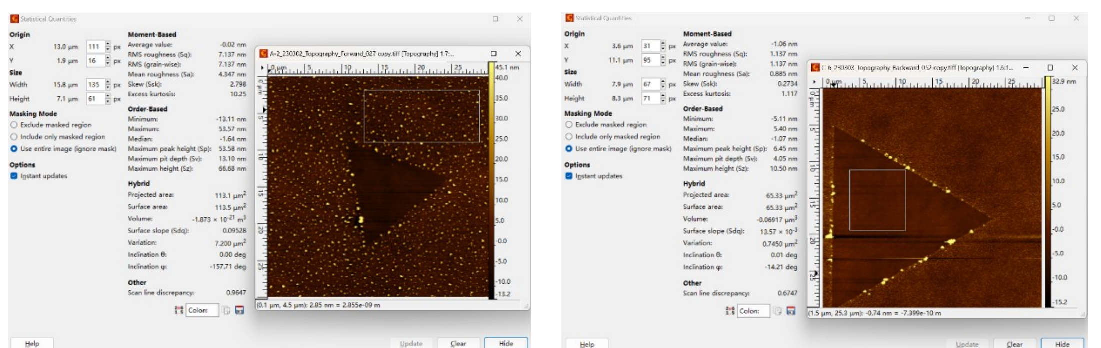

(c) (d)

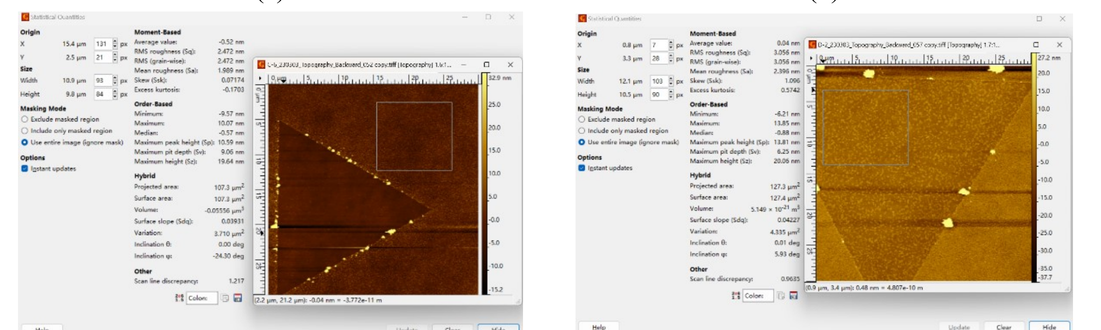

(e) (f)

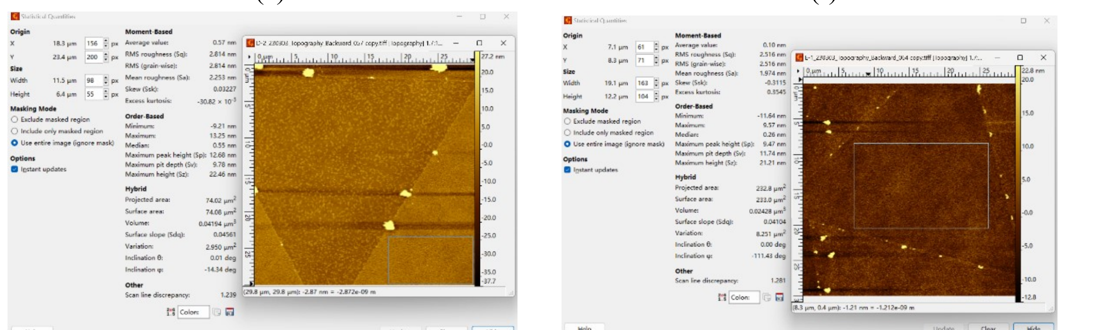

(g) (h)

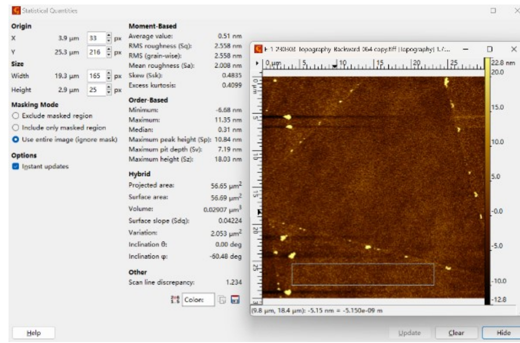

(i)

Fig. S1 Roughness of WS_2 on Si/SiO_2 (a), 10nm $CsSnBr_3$ on WS2 (b) on Si/SiO_2 (c), 30nm $CsSnBr_3$ on WS_2 (d) on Si/SiO_2 (e), 50nm $CsSnBr_3$ on WS_2 (f) on Si/SiO_2 (g), 70nm $CsSnBr_3$ on WS_2 (h) and on Si/SiO_2 (i)

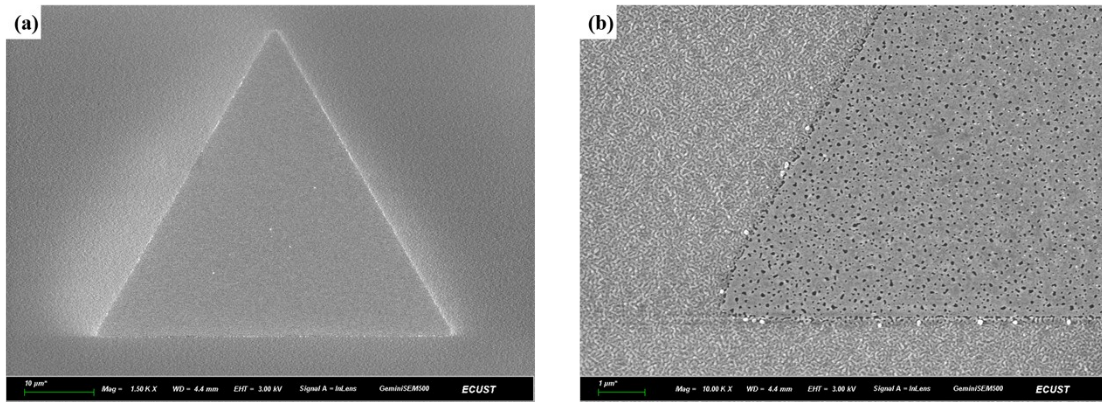

Fig.S2 FESEM images of 10nm $CsSnBr_3$ on WS_2 on Si/SiO_2 (a) × 1500 and (b) × 10000.

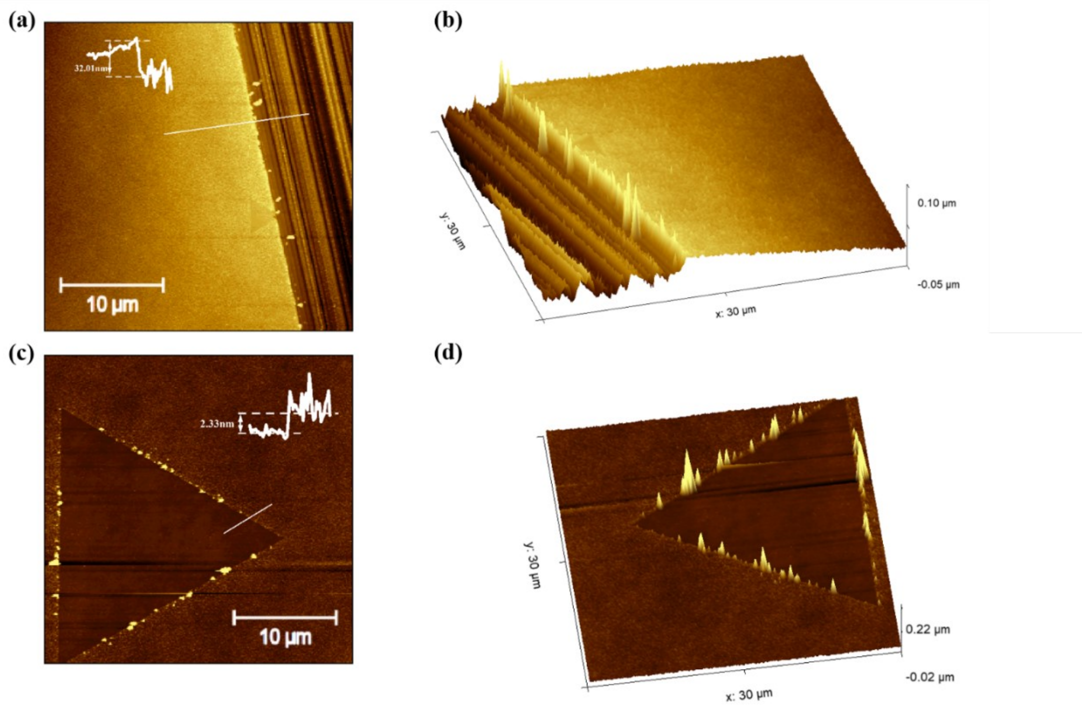

Fig.S3 AFM images of 30nm $CsSnBr_3$ on Si/SiO_2 (a) top view, (b) 3D image, height profile measured along the white line; AFM images of 30nm $CsSnBr_3$ on monolayer WS_2 (c) top view, (d) 3D image.

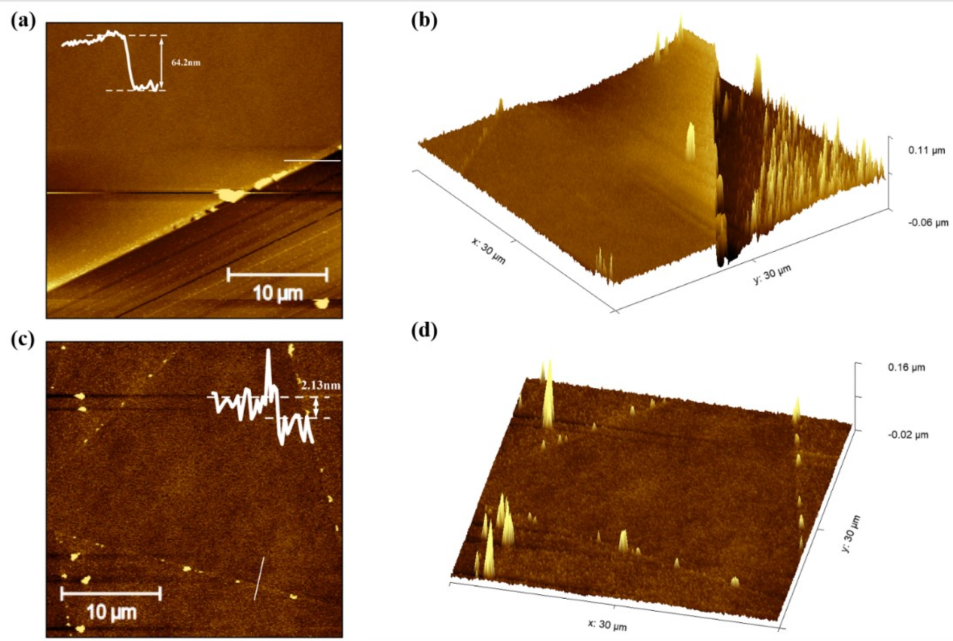

Fig.S4 AFM images of 70nm $CsSnBr_3$ on Si/SiO_2 (a) top view, (b) 3D image, height profile measured along the white line; AFM images of 70nm $CsSnBr_3$ on monolayer WS_2 (c) top view, (d) 3D image

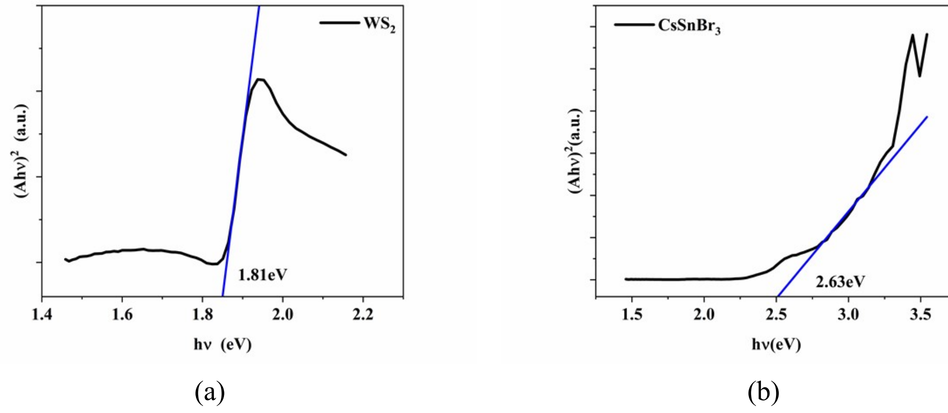

(a) (b)

Fig.S5 Taucs' plot of monolayer WS_2 and 70nm $CsSnBr_3$ on quartz.

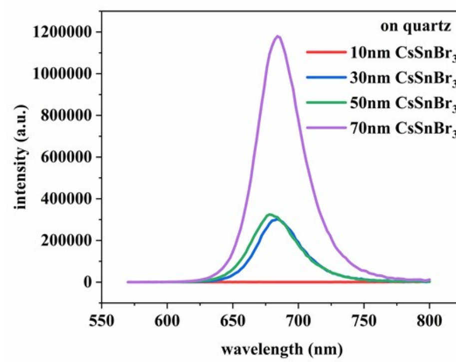

Fig.S6 PL of $CsSnBr_3$ with various thickness on Si/SiO_2

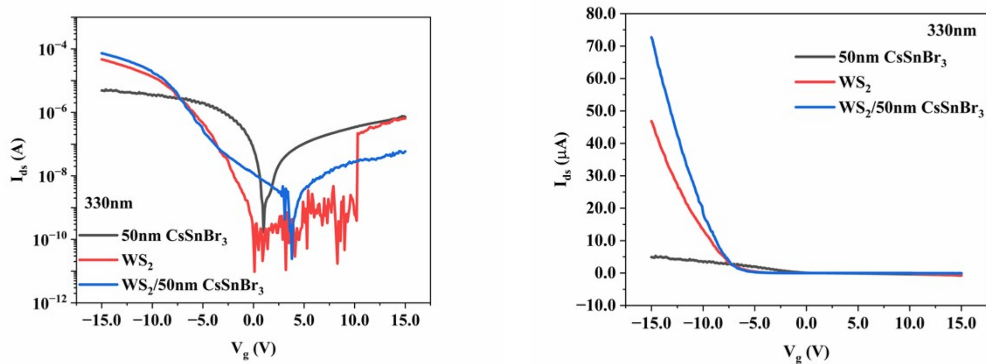

(a)

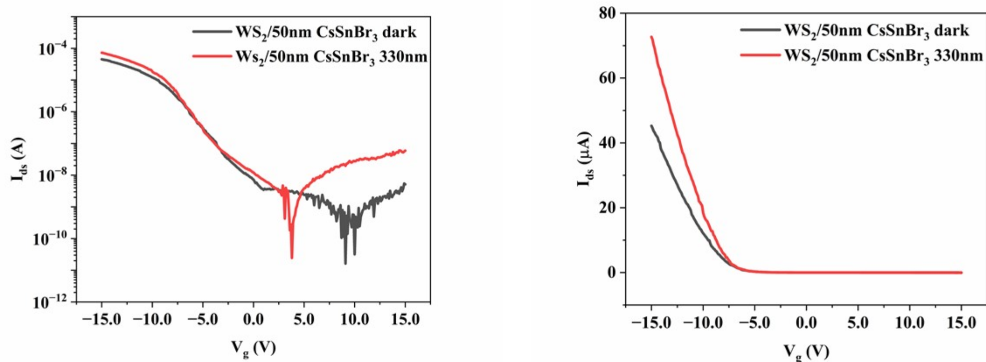

(b)

Fig.S7 Transfer curves of isolated WS_2 and $CsSnBr_3$, and the heterostructure of WS_2/50nm $CsSnBr_3$ at 330nm photo-excitation condition in logarithm and linear scale (a); Transfer curves of the heterostructure WS_2/50nm $CsSnBr_3$ at dark and 330nm photo-excitation conditions in logarithm and linear scale (b).

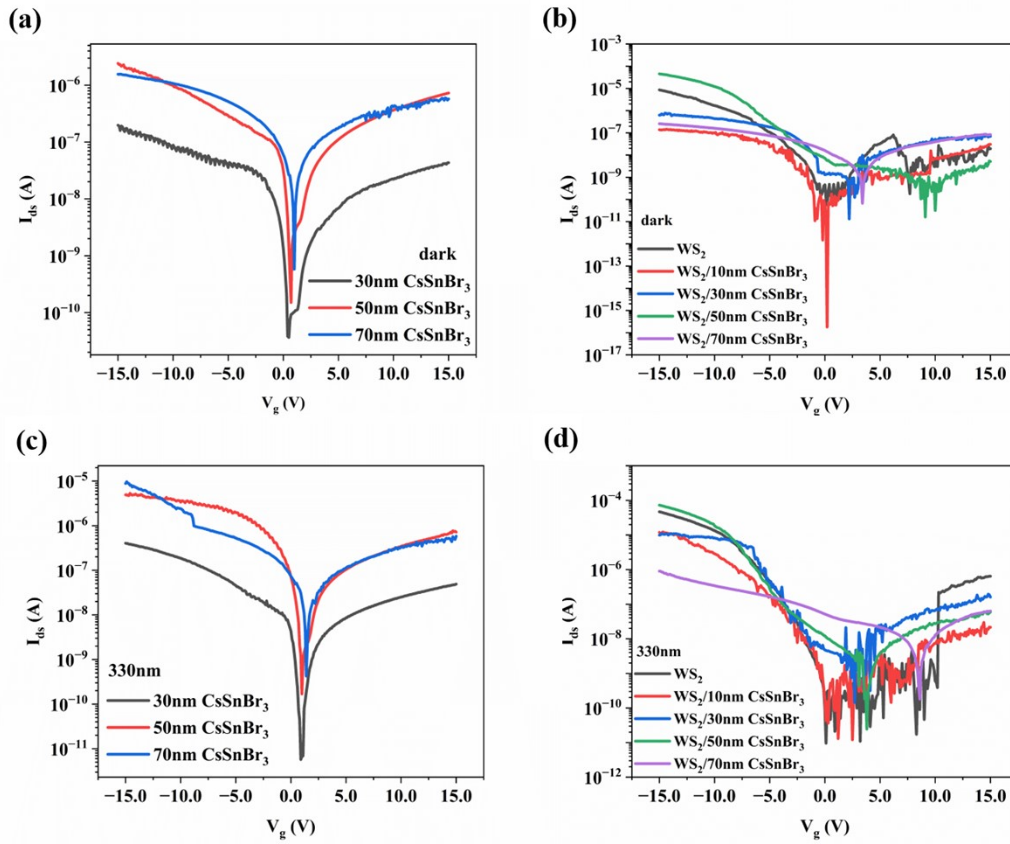

Fig.S8 Transfer curves of isolated $CsSnBr_3$ and the heterostructures of $WS_2/CsSnBr_3$ with various $CsSnBr_3$ thicknesses at dark (a) (b) and 330nm photo-excited (c) (d) conditions in logarithm scale

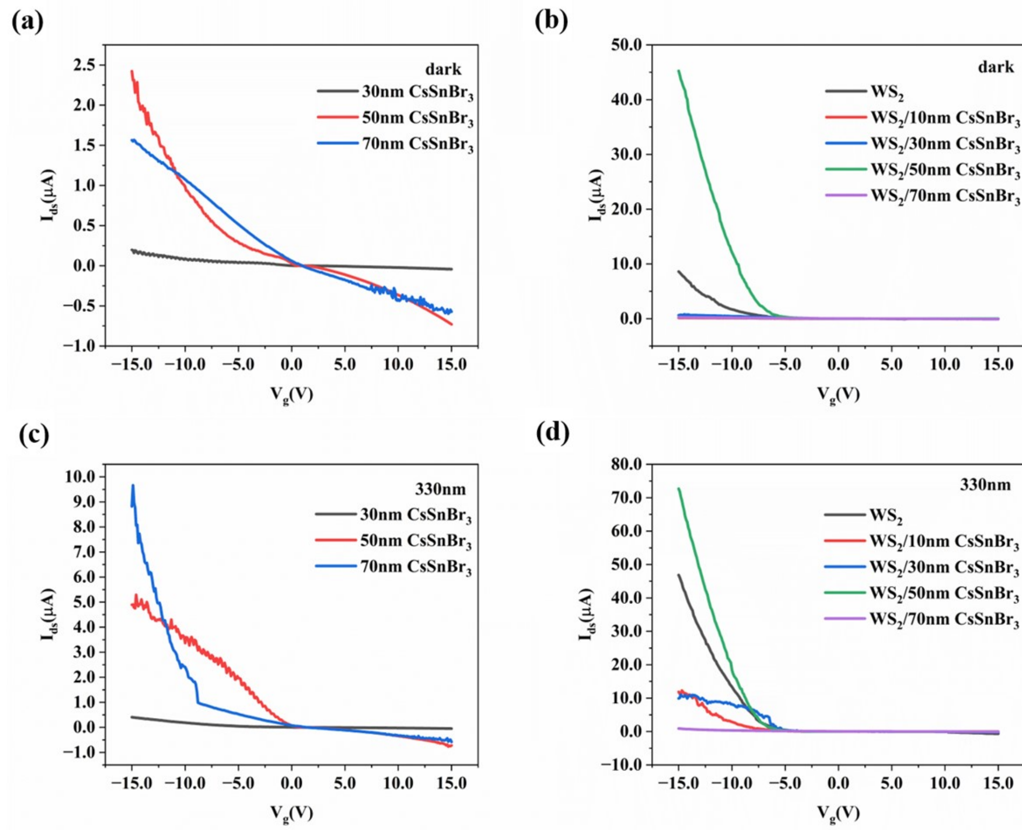

Fig.S9 Transfer curves of isolated $CsSnBr_3$ and the heterostructures of $WS_2/CsSnBr_3$ with various $CsSnBr_3$ thicknesses at dark (a) (b) and 330nm photo-excited (c) (d) conditions in linear scale

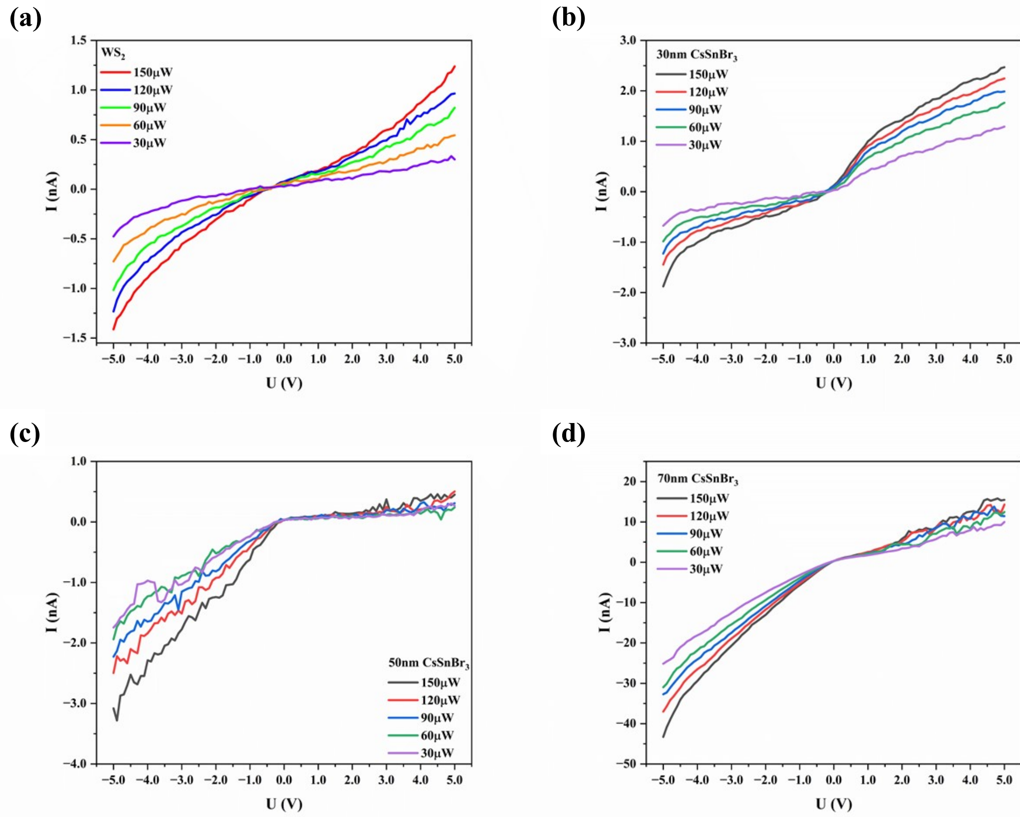

Fig.S10 I_{ph}-optical power at the wavelength of 330nm for (a) monolayer WS_2, (b)30nm, (c)50nm and (d) 70nm $CsSnBr_3$ on Si/SiO_2

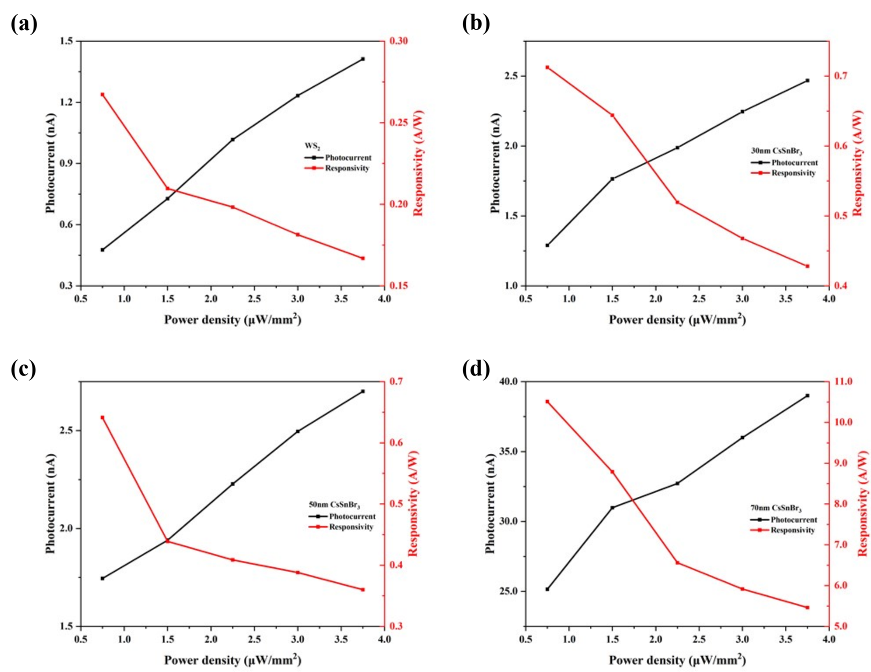

Fig.S11 Dependence of responsivity (R) and I_{ph} on optical power at the wavelength of 330nm for (a) monolayer WS_2, (b)30nm, (c)50nm and (d) 70nm $CsSnBr_3$ on Si/SiO_2

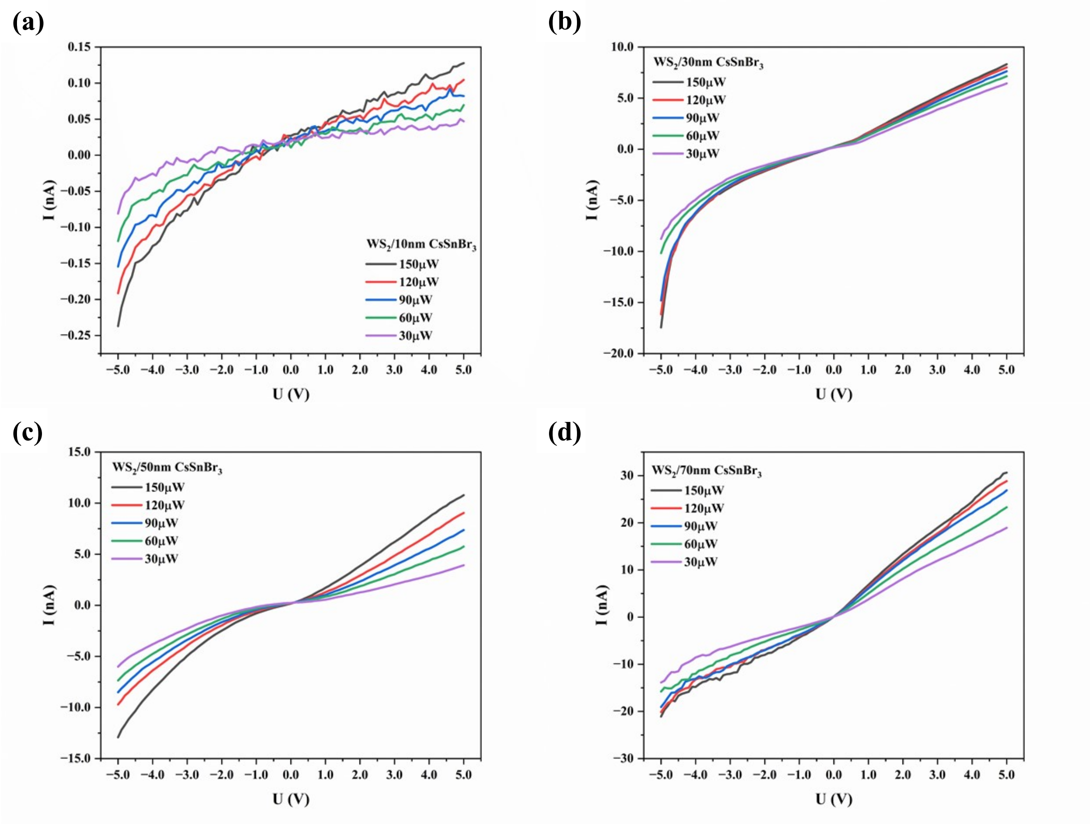

Fig.S12 I_{ph}-optical power at the wavelength of 330nm for the heterostructures of $WS_2/CsSnBr_3$ with $CsSnBr_3$ thickness of (a) 10nm, (b)30nm, (c)50nm, (d) 70nm

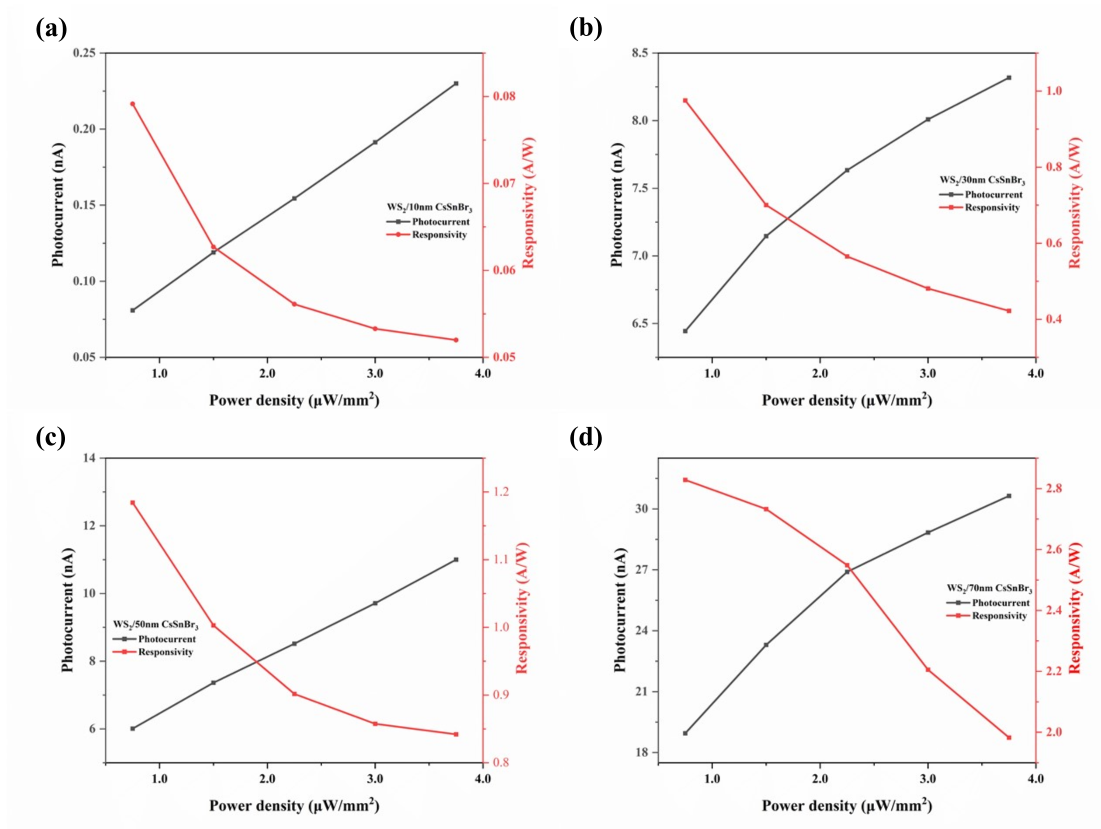

Fig.S13 Dependence of responsivity (R) and I_{ph} on optical power at the wavelength of 330nm for the heterostructures of $WS_2/CsSnBr_3$ with $CsSnBr_3$ thickness of (a) 10nm, (b)30nm, (c)50nm, (d) 70nm

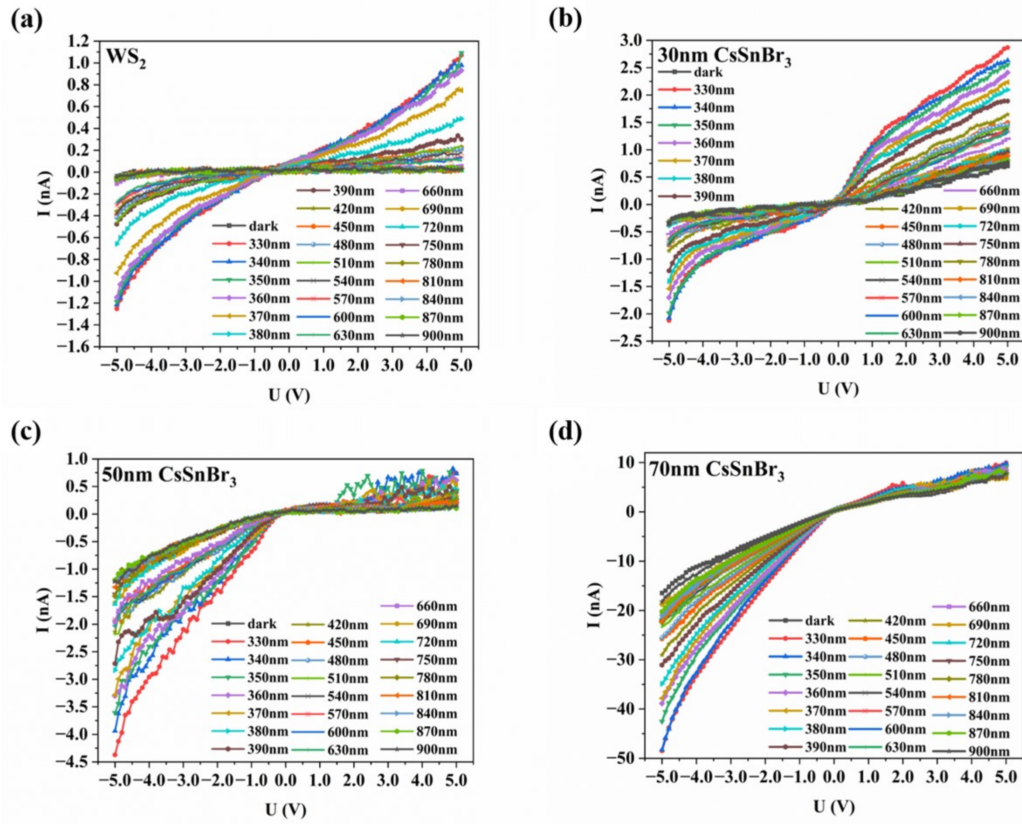

Fig.S14 I_{ph}-wavelength under the optical power of 0.6μw/mm^2 for (a) monolayer WS_2, (b)30nm, (c)50nm and (d) 70nm $CsSnBr_3$ on Si/SiO_2

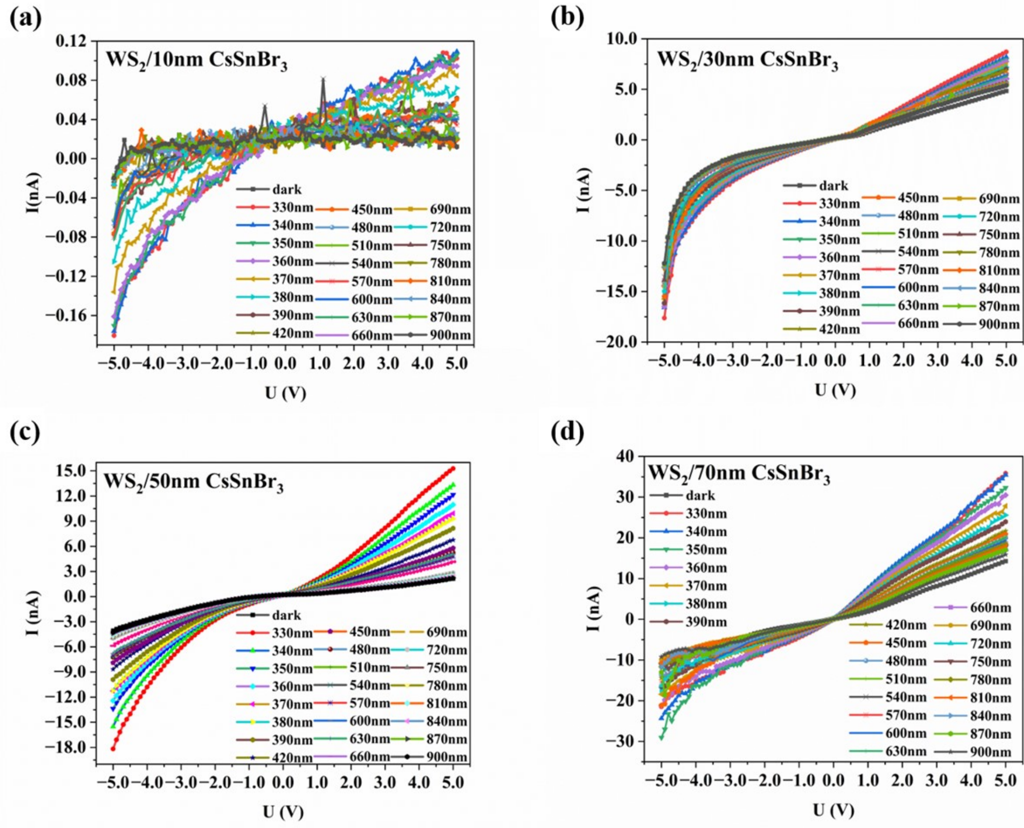

Fig.S15 I_{ph}-wavelength under the optical power of 0.6μw/mm^2 for the heterostructures of $WS_2/CsSnBr_3$ with $CsSnBr_3$ thickness of (a)10nm, (b)30nm, (c)50nm and (d)70nm

Table.S1 Comparison of our work with previously reported Sn-based perovskite photodetector

Sensing materials	Response wavelength (nm)	Responsivity (A/W)	D* (× 10^{10} cmW^{-1}Hz$^{1/2}$)	Response time (ms)	ref
$MASnI_3$ NWs		0.47	8.80 × 10^5	1500/400	1
$MAPb_{0.5}Sn_{0.5}I_3$	905	0.514	1.50 × 10^{11}		2
$CsSnI_3$ NWs	940	0.054	3.85 × 10^{10}	83.8/243.4	3
$CsSnI_3$	850	0.257	1.5 × 10^{11}	0.35/1.6	4
$CsSnI_3$/BMIMCI	405	0.237	1.18 × 10^{12}	0.23/0.19	5
50nm $CsSnBr_3$	330	0.36	8.62 × 10^{10}	340/470	This work
WS_2/50nm $CsSnBr_3$	330	1.62	2.11 × 10^{11}	150/620	This work

Fabrication Procedure

CVD growth of WS_2

The WS_2 nanosheets are fabricated by the chemical vapor deposition (CVD) processing on Si/SiO_2 substrate in a multitemperature zone tubular furnace as depicted in Fig.1(a). The Si/SiO_2 substrates are beforehand ultrasonically cleaned by the acetone, isopropyl alcohol (IPA) and deionized (DI) water subsequently, and then dried by pure nitrogen (N_2) to ensure the crystallization quality of WS_2 nanosheets. 0.4 g Sulphur powder is placed in the position of the center and near inlet gas entrance of the quartz tube which is filled with the inert nitrogen gas under a constant flow (80 sccm). N_2 gas was serviced as the carrier gas. In the high temperature zone, the 40 mg WO_3 and 8mg NaCl are mixed in a sapphire boat along with the Si/SiO_2 substrate placed upside down on it at the downstream. For growth of WS_2 nanosheets, two temperature zones are heated to the temperature of 150 and 830°C, respectively. The size of the as-prepared WS_2 nanosheets can be tuned by the reaction time, which is varied from 5 to 20 minutes. The pressure inside was maintained at 4×10^4 Pa, and then the furnace was naturally cooled down to the room temperature.

Thermal evaporation of $CsSnBr_3$

The $CsSnBr_3$ perovskite films are fabricated by the co-evaporation of the CsBr and $SnBr_2$ source materials simultaneously in a multisource thermal evaporator (LiNing 386SA organic multisource thermal evaporation system, Shenyang, China). The base vacuum of the chamber was kept at 2×10^{-4}Pa. The $CsSnBr_3$ films are annealed at the temperature of 75°C during the thermal evaporation process, namely the in-situ annealing is performed to form the crystalline $CsSnBr_3$. The thickness of the $CsSnBr_3$ films can be monitored by the separated quartz crystal oscillators.

Device Fabrication

Photoresist was spin-coated on as-grown WS_2 as mask. Photoresist patterns for electrodes were conducted through UV photolithography and development. After that, metal electrodes, Ag were deposited by using thermal evaporator and finally lifted off using remover. Then the as-fabricated electrodes were cleaned by DI water and dried by pure nitrogen. The electrodes were subsequently annealed at 350°C in N_2 for 30 min to reduce the contract resistance. Finally, CsBr and $SnBr_2$ were deposited to obtain $WS_2/CsSnBr_3$ devices. The diagram of the formed heterostructure photodetectors is shown in Fig(1) with the Ag electrodes on Si/SiO_2 substrates whose width and length of the channel are kept at 20 and 100μm.

1 A. Waleed, M. M. Tavakoli, L. L. Gu, Z. Y. Wang, D. Q. Zhang, A. Manikandan, Q. P. Zhang, R. J. Zhang, Y. L. Chueh and Z. Y. Fan. *Nano Lett*. 2017, **17**, 523-530.

2 J. M. Wu, Y. Q. Zhang, S. Yang, Z. L. Chen and W. Zhu. *Front. Chem*. 2022, **9**, 821699.
3 M. M. Han, J. M. Sun, M. Peng, N. Han, Z. H. Chen, D. Liu, Y. A. Guo, S. Zhao, C. X. Shan, T. Xu, X. T. Hao, W. D. Hu and Z. X. Yang. *J. Phys. Chem. C*. 2019, **123**, 17566-17573.
4 F. R. Cao, W. Tian, M. Wang, M. Wang and L. Li. *InfoMat*. 2020, **2**, 577-584.
5 Z. Gao, H. Zhou, K. L. Dong, C. Wang, J. Y. Wei, Z. Li, J. S. Li, Y. J. Liu, J. Zhao and G. J. Fang. *Nano-Micro Lett*. 2022, **14**, 215.